Ab initio study of foreign interstitial atom (C, N) interactions with intrinsic point defects in α-Fe

C. Domain
Electricité De France, Recherche et Développement, Matériaux et Mécanique des Composants, Les Renardières, F-77250 Moret sur Loing, France

C. S. Becquart and J. Foct
Laboratoire de Métallurgie Physique et Génie des Matériaux, Ecole Nationale Supérieure de Chimie de Lille, UMR 8517, Centre National de la Recherche Scientifique, Université des Sciences et Technologies de Lille, Electricité De France, Bâtiment C6, F-59655 Villeneuve d'Ascq Cedex, France

(Received 12 December 2003; published 19 April 2004)

The behavior of carbon and nitrogen atoms in iron based solid solution is studied by *ab initio* density-functional-theory calculations. The interaction of a C or a N atom in α-Fe with a vacancy, other C or N interstitials as well as self-interstitial atoms is discussed and compared to known experimental results. The migration of these two foreign interstitial atoms is determined in pure Fe or when a vacancy is present in the supercell. According to our results, there is a strong binding energy of C or N with vacancies, whereas a repulsion is observed with self-interstitial atoms. Furthermore, a vacancy can trap up to two C, and a covalent bonding forms between the two C atoms. The situation is not as clear for N atoms, and a competition between the formation of N-V pairs and NN-V triplets is very probable.

DOI: 10.1103/PhysRevB.69.144112 PACS number(s): 61.72.Ji, 71.15.Mb, 71.20.Be

I. INTRODUCTION

Carbon and nitrogen atoms are the most frequent foreign interstitial atoms (FIA's) in the Fe matrix along with hydrogen atoms. Above their solubility limit, they are responsible for the formation of carbides or nitrides very useful in improving the strength and hardness of steels. Below their solubility limit, the presence of even a very little amount of these impurities in interstitial positions (a few tens ppm) can have a drastic influence on the steel properties, as they build strong interactions with the lattice defects present in the steel. A typical example is the origin of the controversy about the vacancy migration energy in Fe. Schaefer *et al.*,[1] on the one hand, measured a value of 1.28 eV, while Vehanen *et al.*, on the other hand, obtained a vacancy migration energy of 0.55 eV.[2] This data scattering very likely results from the difficulty to obtain very pure Fe crystals.[3] Impurity atoms, even in very small amount, trap the vacancies and thus decrease the vacancy diffusion coefficient. Indeed the much smaller value of 0.55 eV was measured for a high purity α-Fe.[2] The C and N atoms can as well interact with extended defects such as dislocations, grain boundaries.

Under irradiation, there is ample evidence that FIA's play a major role in the various damage processes in α-Fe and ferritic steels, because of the strong interactions they have with point defects (for a thorough review, see for instance the review paper by Little[4]). For instance, it has been observed that interstitial nitrogen enhances the radiation hardening either by increasing the defect-loop density and/or by stabilizing small faulted $\langle 110 \rangle$ loops.[5] The results of internal friction work[6] and those of resistivity measurements[7] also indicate that carbon being trapped by radiation-produced defects was being removed from the solid solution and precipitation of carbides was hindered.

Although the nature of the interactions between the interstitial solutes and the self-interstitial atom (SIA) produced by irradiation is not completely understood yet, it appears that irradiation affects the behavior of the FIA's either by providing nucleation sites and thereby enhancing the rate of precipitation or by introducing defects or defect clusters which trap the FIA's.

Computer simulations at the atomistic level, such as molecular dynamics, are ideal tools to study the interactions of impurities with point defects. However the accuracy of the results depends very much on the cohesive model used. The empirical potentials are most of the time parametrized on equilibrium properties (elastic constants, vacancy formation energies, and so on) but they do not always reproduce correctly properties related to the short-distance interaction range, such as the so-called interstitial region. For instance, three embedded atom method potentials considered in the literature as being representative of α-Fe were investigated[8] and led to predict very large differences in the interstitial formation energies. Furthermore, the results obtained were also different from those predicted by a Finnis-Sinclair-type potential derived by Ackland and co-workers.[9]

Some FeC semiempirical potentials have been derived in the past.[10–12] Johnson[10] derived two-body central potentials for the FeC system. The metal-metal and the metal-carbon interactions are described by pairwise potentials (it is now widely agreed that pairwise interactions alone are not appropriate to model metal-metal interactions), and no carbon-carbon interactions are assumed. The Fe-C interaction potential was constructed such that the experimental carbon migration energy in Fe, and the activation volume for that migration, as well as the binding energy of a carbon vacancy dipole were reproduced by the model.

Rosato[11] used a more realistic potential for Fe, based on the tight-binding second-moment approximation, achieving a better calculation of elastic properties and a more natural agreement with experimental data. For the metal-metal potential he used for α-Fe a Finnis-Sinclair model,[13] for γ-Fe a

Rosato-Guillope-Legrand.[14] The carbon-metal interaction is also described by a pair potential, and as the author aimed at studying the behavior of a single C atom, he did not derive any carbon-carbon interaction.

More recently, Ruda *et al.*[12] derived an embedded atom method potential for FeC even though C-C interactions are not accurately considered when angular terms are neglected. The potentials were adjusted on *ab initio* calculations from the literature of the metastable carbide FeC in the B1 structure. The authors reproduced the equilibrium lattice constant, the bulk modulus, and the cohesive energies for each of the stable and metastable carbides.

Even though the potentials improved over the years, their accuracy is still a matter of controversy specially regarding fine properties related to the interactions of C or N atoms with point defects. *Ab initio* calculation based on the density-functional theory is today the most appropriate tool to evaluate these fine interactions and as a consequence to understand better the basic atomic phenomena involved.

Several *ab initio* studies have been dedicated to the determination of structural parameters, electronic structures, and magnetic properties of carbides and nitrides, either stable or metastable, however much less effort has been put on investigating C or N in solid solution in Fe.

In this work, the interaction of C and N in the Fe bcc matrix as well as their interaction with vacancy and interstitial is revisited. When relevant, comparisons are made between our results and data predicted by empirical interatomic potentials.

The paper is organized as follows: after the presentation of the calculation method used, we present in a first part the FIA most favored position in the α-Fe matrix and determine its diffusion coefficient. In a second part, we discuss the strength of the FIA interactions with various point defects: vacancy (V), FIA of same nature, FIA-V complexes, and self-interstitial atoms to finally conclude on the possible effects of C or N on intrinsic point defects of the α-Fe matrix.

II. METHODOLOGY

Ab initio calculations based on the density-functional theory[15] have now demonstrated their capability to treat large enough number of atoms for investigating a broad field of problems in materials science.[16] Our calculations have been performed using the Vienna *ab initio* simulation package (VASP).[17–19] The calculations were performed in a plane-wave basis, using fully nonlocal Vanderbilt-type ultrasoft pseudopotentials to describe the electron-ion interaction.[20] Exchange and correlation were described by the Perdew and Zunger functional,[21] adding nonlocal correction in the form of the generalized gradient approximation (GGA) of Perdew and Wang.[22] All the calculations were done in the generalized gradient approximation within the spin-polarized formalism. The ultrasoft pseudopotentials were taken from the VASP library. For Fe, the six $3d$ electrons are considered as valence ones together with the two $4s$ (the reference state is more precisely $3d^{6.2}4s^{1.8}$). For C, four valence electrons are used: $2s$ and $2p$ (reference $2s^2 2p^2$). For N, five valence electrons are used: $2s$ and $2p$ (reference $2s^2 2p^3$). In addition, some calculations were done using the projector augmented wave (PAW) approach[23] as well as taking into account the corrections of Vosko and co-workers for the exchange correlation.[24]

The supercell approach with periodic boundary conditions was used to simulate point defects as well as pure phases. Brillouin-zone sampling was performed using the Monkhorst and Pack scheme.[25] The ion relaxations were performed using the standard conjugate gradient algorithms implemented in the VASP code. They were done at constant volume thus relaxing only the atomic position in a supercell dimensioned with the equilibrium lattice parameter for Fe (2.8544 Å). This allows one to use a smaller plane-wave energy cutoff of 240 eV for the calculations involving nitrogen atoms and 290 eV for those involving carbon atoms. The relative error induced by this lower-energy cutoff was checked to be negligible, as can be seen later in text and in our previous work.[26] In all the results presented here, the number of k points is the total number of k points (not the number of irreducible k points which depends on the supercell symmetry). In all the tables presented below, the ''number of atoms'' is more precisely the number of metal sites in the perfect supercell, i.e., the cell without any defects.

The formation enthalpy is calculated taking as reference the isolated atoms rather than the stable states of C and N. The values obtained differ from the experimental data by a constant value. For a supercell containing N Fe atoms and one FIA, the formation enthalpy, ΔH_f^{FIA}, is calculated as follows:

$$\Delta H_f^{\mathrm{FIA}}(\mathrm{Fe}_N\mathrm{FIA}) = E(\mathrm{Fe}_N\mathrm{FIA}) - NE(\mathrm{Fe}) - E(\mathrm{FIA}_{isolated}), \tag{2.1}$$

where $E(\mathrm{Fe})$ is the reference energy of bulk Fe with the same structure (bcc) than in Fe_NFIA, and $E(\mathrm{FIA}_{isolated})$ is the energy of the C or N isolated (a single C or N alone in a large supercell).

The binding energies between two entities in a bcc iron matrix are calculated as follows. The binding energy $E_b(A_1,A_2)$ is defined as the difference of two system energies $E_{noninterac}$ and $E_{interac}$:

$$E_b(A_1,A_2) = E_{noninterac} - E_{interac}. \tag{2.2}$$

In system *noninterac*, A_1 and A_2 do not interact, i.e., they are situated far enough from each other not to interact. In system *interac*, A_1 and A_2 interact, and the distance between A_1 and A_2 may be first nearest-neighbor distance, second nearest distance, and so on.

Because of the relatively small supercell sizes one may use, it is rather difficult to make sure that the two entities in system *noninteract* do not interact even when they are as far as the supercell size allows. Another method can be used to determine the binding energies which consists in subtracting from the energy of system *interact* (where A_1 and A_2 interact), the energy of a system containing A_1 (calculated with a supercell with a size similar to that of system *interact*) as well as that of a system containing A_2 (obtained with similar

conditions) and that of the supercell with neither A_1 nor A_2. For a supercell containing N atoms, the binding energy is thus obtained as

$$E_b(A_1,A_2)=[E(A_1)+E(A_2)]-[E(A_1+A_2)+E_{ref}], \tag{2.3}$$

where E_{ref} is the energy of the supercell without A_1 and A_2, $E(A_1)$ [respectively $E(A_2)$] is the energy of the supercell with A_1 (respectively A_2), $E(A_1+A_2)$ is the energy of the cell containing both A_1 and A_2 interacting, i.e., the energy of system *interact* in the previous method. All the supercells contain the same number of sites, i.e., have the same size.

For more than two interacting entities, Eq. (2.3) can be generalized as follows:

$$E_b(A_1,\ldots,A_n) = \left[\sum_1^n E(A_i)\right]-[(n-1)E_{ref}+E(A_1+\cdots+A_n)]. \tag{2.4}$$

Except when otherwise stated, the reference state of the binding energies presented in this work is always the energy of a supercell without any entities, i.e., a perfect crystal. With such a scheme a positive binding energy means attraction between the entities, while a negative binding energy indicates a repulsion. This definition will be used to explore various scenarios for the formation of small FIA-V complexes.

The electronic structure of the Fe-C and Fe-N interaction has been analyzed using the density of states as well as the electronic density deformation map. In order to calculate local quantities such as the local density of states or the local magnetic moment, it is necessary to introduce atomic radii to proceed to local projection on some orbitals (s, p, and d). The values adopted throughout this work are the recommended ones for the VASP code: 1.302 Å for Fe, 0.863 Å for C, and 0.783 Å for N. The Fermi energy has been taken as the zero of energy in all the figures representing the density of states.

For a supercell (Fe_iX_j) containing i Fe atoms and j X atoms (where X stands for C or N) the electronic density deformation map due to the presence of atoms of type X is obtained by subtracting from the electronic density of (Fe_iX_j) both the electronic density of (Fe_i) and the electronic density contribution of each isolated (X_k):

$$\Delta\rho=\rho(Fe_iX_j)-\rho(Fe_i)-\sum_{k=1,j}\rho(\text{atom } X_k \text{ isolated}). \tag{2.5}$$

(Fe_i) is the supercell where all the X atoms have been removed, and (X_k) is isolated in the same supercell. In this scheme, isosurfaces of the deformation map give a direct real-space visualization of the local electronic rearrangements due to the presence of the X atom(s).

The distortion due to the presence of the FIA has been characterized by determining the dipolar tensor from the Kanzaki forces. The Kanzaki forces are the forces that when applied to the perfect lattice would produce the same displacements that the defect does. They thus, to a first approximation, represent the forces with which the FIA interacts with its neighboring Fe atoms. The calculation procedure, derived by Simonelli *et al.*,[27] is as follows: once the bcc Fe lattice with the FIA has been fully relaxed, the FIA is removed from the supercell. The forces on all the Fe atoms are then calculated. These forces are the Kanzaki forces. The dipolar tensor P is then obtained from the Kanzaki forces: $P^{\alpha\beta}=\Sigma r_j^\alpha k_j^\beta$. j is taken within a sphere of radius R centered on the former FIA position, k_j^β is the Kanzaki force on atom j in the β direction, and r_j^α is the αth component of the vector joining atom j and the FIA. The defect relaxation volume is given by the trace of the dipolar tensor: $\Delta V=\mathrm{Tr}(P)/3B$ where B is the bulk modulus.

In our case, we restricted the inside region[27] to the FIA only. Furthermore we assumed that the displacements of all the iron atoms were in the harmonic regime. Although, this approximation is not totally correct for the Fe atom first nearest neighbors of the FIA, it gives an estimate of the dipolar tensor. In any case, as the simulation supercells are quite small, approximate values only can be expected.

TABLE I. Different crystallographic structures investigated for C (full relaxation calculation with an energy cutoff of 350 eV) and N (full relaxation calculation with an energy cutoff of 240 eV).

State of C	C cohesive energy (eV)	State of N	N cohesive energy (eV)
Graphite ($c=7.46$ Å)	−11.256	N_2 molecule	−3.995
Graphite ($c=11.246$ Å)	−11.246		
Diamond	−11.166		

III. INTRODUCTION OF A SINGLE FIA IN bcc Fe

A. Pure elements

Bulk properties obtained with VASP for pure iron with or without substitutional Cu atoms have been investigated in detail in our previous work.[26] At 0 K, our calculations are consistent with the experimental results. The ground state of Fe is magnetic bcc as is observed experimentally [$T_{Curie}=1043$ K (Ref. 28)] with an equilibrium lattice parameter of 2.8544 Å and a mean magnetic moment of $2.32\mu_B$/atom. As observed by Kresse and Joubert,[29] the magnetization is overestimated by $0.1\mu_B$/atom compared to the experimental results.[28] The local magnetic moment after projection of the electronic density on the sphere centered on the atom (whose radius is the radius used for local density of state projection) is $2.37\mu_B$/atom. The slight difference between the mean magnetic moment and the local magnetic moment comes probably from the overlap of the spheres.

For C and N, we determined the cohesive energies for different possible crystallographic structures as well as for the isolated atoms. The results are reported in Table I. For C, the graphite structure was found to be the most stable. As it is now commonly agreed on that the interlayer van der Waals interactions are not correctly described within the density-

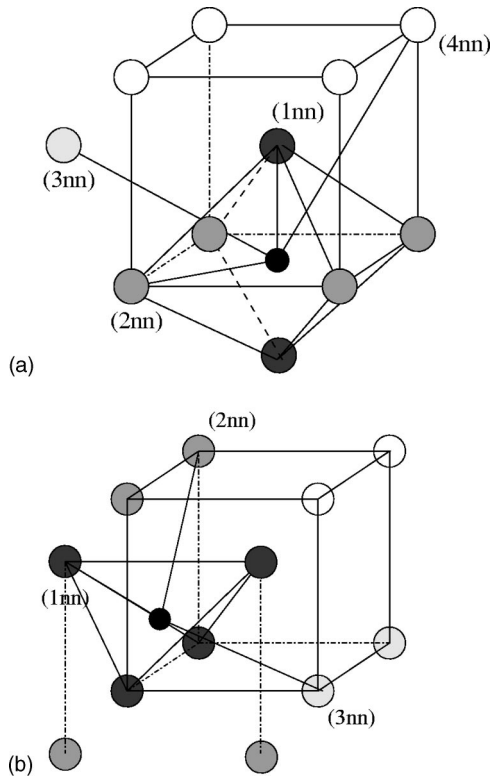

FIG. 1. Interstitial sites and their Fe neighbor atoms in bcc Fe. (a) Octahedral, (b) tetrahedral. The FIA is represented by a small black sphere, its first nearest neighbor by a large black sphere, its second nearest neighbor in gray, the other neighbors are represented by large white spheres. 1nn stands for first nearest neighbor, 2nn stands for second nearest neighbor and so on.

functional theory, we calculated the cohesive energies when the interlayer distance is the experimental distance, i.e., 6.80 Å as well as for the most stable structure predicted by VASP which leads to an interlayer distance c of 7.46 Å. The discrepancy between the real structure of graphite and the one predicted by VASP affects the energy by only 10 meV which is small compared to the energy difference between diamond and graphite. This indicates that the most significant contribution to the cohesive energy comes from the interactions within the graphite layers rather than from the weak interactions between layers. The diamond phase was found to have a lattice parameter of 3.584 Å. For N, the N_2 molecule is the most stable with an equilibrium distance of 1.214 Å.

B. Single FIA in bcc Fe

1. Energetics

In transition metals, small foreign atoms usually sit on interstitial sites. In the bcc structure, two types of sites are possible, octahedral or tetrahedral sites. These sites are represented in Fig. 1. Larger foreign atoms usually sit on a regular lattice site (which will be here referred to as the substitutional configuration) or as part of mixed dumbbells: two atoms sharing a regular lattice site. Table II summarizes the formation enthalpies per FIA when the impurity atoms are positioned in different configurations. The formation energies are relative to the reference state chosen, here the isolated atoms.

For both C and N atoms, the most stable position is the octahedral (O) site in agreement with the most common interpretation of the experimental observations[30] and Rosato's[11] simulations. The more recent simulation of Ruda *et al.*[12] disagrees with these results as they predict the tetragonal site to be the most stable for C.

The energy difference between both interstitial sites is an important parameter related to the migration energy of carbon and nitrogen in the bcc Fe. In this work, the tetragonal site was found to be the saddle point for migration, situated halfway between two octahedral sites. By looking at the dynamical matrix, when in tetrahedral position, it was verified that the tetragonal site is indeed a saddle point and not a local minimum. Consequently the migration energy of C or N is equal to $\Delta E[(T)-(O)]$.

The influence of the ion-electron interaction scheme (ultrasoft pseudopotentials versus projector augmented wave) and the effect of the Vosko correction on the results have been checked in the case of the C migration energy. The Vosko correction with the ultrasoft pseudopotential gives 0.94 eV for $\Delta E[(T)-(O)]$ for C in a 54-atom supercell calculation leading to a 10 meV difference with ultrasoft pseudopotentials (see Table II), while when one uses the projector augmented wave scheme (not taking into account the

TABLE II. Formation enthalpies for a single C atom or a single N atom positioned in the two possible interstitial sites, in a substitutional configuration, or as a mixed dumbbell (in eV). The reference state for the FIA is the isolated atom. The calculations were done using 54-atom supercells and 125 k points as well as 128-atom supercells with 27 k points. (O) means that in the course of the ionic relaxation, the impurity spontaneously relaxes to an octahedral site.

Configuration	C (54 atoms)	C (128 atoms)	N (54 atoms)	N (128 atoms)
Substitutional	−8.742	−8.094	−2.387	−2.219
Tetrahedral (T)	−9.787	−9.557	−4.407	−4.342
Octahedral (O)	−10.710	−10.459	−5.196	−5.107
$\Delta E[(T)-(O)]$	0.923	0.902	0.789	0.765
Mixed ⟨100⟩ interstitial	(O)	(O)	(O)	(O)
Mixed ⟨110⟩ interstitial	(O)	(O)	(O)	(O)
Mixed ⟨111⟩ interstitial	−9.139		−3.379	

TABLE III. Plane-wave energy cutoff effect on C and N migration energies. The calculations were done using 54-atom supercells and 125*k* points.

C		N	
Energy cutoff (eV)	$\Delta E[(T)-(O)]$ (eV)	Energy cutoff (eV)	$\Delta E[(T)-(O)]$ (eV)
		240	0.789
290	0.923	300	0.788
350	0.924	350	0.789

Vosko correction) the C migration energy becomes 0.79 eV leading to a 0.1 eV difference with the ultrasoft pseudopotential scheme.

Our results are in very good agreement with the experimental data. The experimental migration energy of C determined by resistivity measurements, positron-lifetime measurements, or Snoek relaxation lies between 0.81 eV and 0.83 eV.[31] However, Takaki and co-workers by resistivity recovery of high purity and C doped iron find a higher value of 0.88 eV (Ref. 32) for a carbon atom in Fe. For a N atom in bcc Fe, the migration energies are lower: between 0.76 eV and 0.80 eV.[31]

Our results indicate that the carbon and nitrogen migration energies are higher than the vacancy migration energy in α-Fe (found to be 0.65 eV in our calculations[26]). This indicates that it is probably a moving vacancy which is trapped by a carbon or a nitrogen atom, rather than a moving impurity trapped at a vacancy in agreement with Vehanen and co-worker's positron-lifetime measurements.[2] Weller and Diehl[33] observed that upon irradiation of α-Fe, the interstitial carbon stays in solution to a somewhat higher temperature than nitrogen, which is consistent with the higher migration energy for C than for N found in these calculations. With his empirical potential Rosato[11] obtains a value of 1.14 eV for the migration energy of a carbon atom, which is not too far from the experimental data. However, with their embedded atom method potential, Ruda *et al.*[12] found a much too low-energy difference between the two interstitial sites (0.1 eV). This potential thus appears not to reproduce very correctly the C migration properties. As far as the convergence of the *ab initio* results with the supercell size is concerned, Table II indicates that the energies are rather well converged compared to the relative values we are interested in.

The low plane-wave energy cutoff used appears not to have a significant effect on the relative energies calculated, as can be seen in Table III which presents the values of the C and N migration energies in bcc Fe obtained for different values of the energy cutoff. The relative error is of the order of 1 meV, which is negligible.

The impurity diffusion coefficient is given by $D=D_0\exp(-E_a/kT)$ where E_a is the activation energy, equal to $E(T)-E(O)$ in this work, and $D_0=\frac{1}{6}a^2\nu$, where a is the lattice parameter and ν the attempt frequency. In the framework of the Vineyard transition state theory,[34] $\nu=\Pi_1^{3N}\nu_i/\Pi_1^{3N-1}\nu_i^*$. ν_i are the vibration modes in the initial configuration [(O) site] and ν_i^* the vibrational modes in the transition state configuration [here the (T) site]. Within the Einstein approximation, only the vibrational modes of the migrating C or N atom need to be considered, which reduces the $3N\times 3N$ matrix into a 3×3 matrix. The matrix elements have been obtained by translating the migrating atom in the three directions by 0.025 Å. The prefactor thus obtained for C is $D_0(C)=2.13\times 10^{-7}$ m^2/s, in good agreement with Carter's calculations[35] which give 1.44×10^{-7} m^2/s for $D_0(C)$. For N, the Einstein approximation gives $D_0(N)=9.42\times 10^{-8}$ m^2/s. These results are in good agreement with the experimental results as can be seen in Table IV.

TABLE IV. C and N diffusion coefficient prefactors and activation energies, calculated with 54-atom supercells and 125 k points.

FIA	Method	Prefactor (10^{-7} m^2/s)	E_a (eV)
C	This work	2.13	0.92
C	*ab initio*[a]	1.44	0.83
C	Expt.[b]	1.67	0.81
C	Expt.[b]	3.94	0.83
N	This work	0.94	0.79
N	Expt.[b]	1.26	0.76
N	Expt.[b]	4.88	0.80

[a]Reference 35.
[b]Reference 31.

This method can also be used to evaluate the prefactor associated to the vacancy diffusion. The prefactor for vacancy diffusion is given by $D_0(V)=fa^2\nu$, with $f\simeq 0.7$. ν was estimated to be equal to 5×10^{13} Hz, thus $D_0(V)=3\times 10^{-6}$ m^2/s. The vacancy diffusion coefficient is thus larger than the FIA diffusion coefficient, which is in agreement with the fact that it is the moving vacancies which come to the FIA's. At thermal equilibrium the vacancy concentration is several orders of magnitude smaller than the FIA concentration in solid solution. Consequently, the vacancies are almost all the time trapped by FIA's, and their effective migration energies are increased if the matrix contains FIA's.

2. Atomic relaxation

The relaxation of the Fe atoms close to the FIA is presented in Table V. The octahedral site being smaller than the tetrahedral one, the relaxation of the Fe atoms is greater in the octahedral site than in the tetrahedral. The relaxation of the Fe atoms around the FIA is very similar whatever the FIA nature. However a slightly smaller relaxation around the N atom than around the C atom is observed, fully consistently with anelastic relaxation measurements[36] and with the FIA atomic radii.

The relaxation of the Fe atoms around the octahedral site for C of Table V is slightly lower than the values obtained by Cochard and co-workers[37] from x-ray measurements of the tetragonal distortion of martensite. However the orders of magnitude and the signs are similar. Rosato's empirical potential[11] leads to a higher relaxation around the C FIA than what is found in this work. Indeed, he obtains $\Delta d_1/d_1^0=+28.7\%$ and $\Delta d_2/d_2^0=-4.7\%$ for a C atom in an octahe-

TABLE V. Relaxation (in percent of $\Delta d_i/d_i^0$) around the FIA in the bcc structure. The third column indicates the number of neighbor atoms situated at distance d_i of the FIA. d_i^0 is the distance between the impurity and the atom before any relaxation, d_i is the new distance between the impurity and the atom after the relaxation. d_1 is the first nearest-neighbor distance, d_2 is the second nearest-neighbor distance. The calculations were done in 54-atom supercells using 125 k points and 128-atom supercells using 27 k points. The model of Cochard and co-workers (Ref. 37) based on measurements of the mean tetragonal distortion of martensite suggests that for the unit cell surrounding the carbon atom $\Delta d_1/d_1^0=38\%$ and $\Delta d_2/d_2^0=-2.6\%$.

Configuration		No. of atoms	C (54 atoms)	C (128 atoms)	N (54 atoms)	N (128 atoms)
Substitutional	d_1	8	−5.0	−4.8	−4.3	−4.4
Substitutional	d_2	6	+1.1	+1.2	+1.9	+2.2
Tetrahedral (T)	d_1	4	+13.7	+13.9	+11.9	+12.0
Tetrahedral (T)	d_2	4	−2.9	−2.9	−0.9	−0.6
Octahedral (O)	d_1	2	+23.8	+24.3	+22.9	+23.4
Octahedral (O)	d_2	4	−1.9	−1.8	−2.0	−1.8

dral site. d_i^0 is the distance between the impurity and the atom before any relaxation, d_i is the new distance between the impurity and the atom after the relaxation. d_1 is the first nearest-neighbor distance, d_2 is the second nearest-neighbor distance. The empirical atomic potential derived by Ruda *et al.*[12] also predicts a strong relaxation around the C atom. However with this potential, the most energetically favored site is the tetrahedral position.

To better characterize the distortion introduced by the FIA in the Fe matrix, the dipolar tensor has been evaluated when the FIA is in an octahedral site. Because of the symmetry of the configuration, the dipolar tensor has two independent values only: P_{11} and P_{33} as $P_{11}=P_{22}$. The results are summarized in Table VI for increasing values of the radius R. Despite the problems in obtaining converged results for the dipolar tensor and the relaxation volume because of the small number of atoms in the supercell, it appears clearly that the dipolar tensor is highly anisotropic. These results are not surprising as in the bcc structure, the coordination polyhedron of the octahedral site is not a regular octahedron as two Fe atoms are situated at $0.5a_0$ from the FIA while the other four atoms of the octahedron are situated at $a_0/\sqrt{2}$ (see Fig. 1). As a consequence, a large value of P_{33} (around 10 eV) is obtained along the direction which contains the two Fe atom first nearest-neighbor to the FIA, while a much smaller value (around 1 eV) is obtained in the plane which contains the four Fe atom second nearest-neighbors to the FIA. No significant difference is observed between C and N.

TABLE VI. Dipolar tensor obtained from the Kanzaki forces determined using 54-atom supercells. R is the radius of the sphere containing the atoms on which the forces are calculated. The number of atoms included in the sphere is also specified.

Configuration	R (Å)	No. of atoms	$P_{11}=P_{22}$ (eV)	P_{33} (eV)	ΔV (Å^3)
C (O)	3	6	1.1	9.2	3.2
C (O)	4	22	2.0	10.5	4.0
C (O)	4.5	32	0.6	10.4	3.2
N (O)	3	6	1.0	8.8	3.0
N (O)	4	22	2.4	10.4	4.2
N (O)	4.5	32	1.0	10.2	3.4

To summarize, the presence of a C atom or a N atom in an octahedral site in bcc Fe leads to a large tetragonal distortion of the lattice, which generates a highly anisotropic strain field, i.e., $\epsilon_{zz} \gg \epsilon_{xx}=\epsilon_{yy}$ very similar whether the FIA is a C or a N atom.

3. Electronic structure and magnetic moment

Figure 2 represents the local density of states of the Fe atom first neighbor to a FIA in an octahedral position as well as the density of states of the FIA itself. A small depletion in the Fe $3d$ states of the density of states is observed as compared to the density of states of pure bcc Fe and a hybridization around −6 eV for C and −7.5 eV for N of the Fe d states with the FIA $2p$ states [situated at around −5 eV for C and at around −7 eV for N (Ref. 38)]. This indicates the formation of an interaction between the FIA and the Fe atoms. The interaction is larger when the Fe atom is first neighbor to the FIA, than when it is second neighbor. When the FIA is a C atom, the peak associated to the hybridization is wider than when it is a N atom indicating a less localized bonding of the C than of the N atom with iron as can be seen in Fig. 3. Because of the interaction with the FIA, the minority-spin d states of the Fe atom first neighbor of the FIA is larger than that of pure bcc Fe, which leads to a decrease of the local magnetic moment on the first nearest-neighbor Fe atoms (about 1.72 μ_B/atom for both C and N as compared with $2.37\mu_B$/atom). The local magnetic moments carried by the matrix atoms as well as the FIA's are summarized Table VII. As the distance between the FIA and the Fe atoms increases, the density of states looks more and more like the density of states of pure bcc Fe. As already observed for the Fe atom relaxations around the FIA, the moments carried by the matrix atoms or the FIA are very similar no matter what the FIA nature is. The local moments appear to depend more on the FIA position (octahedral site rather than tetrahedral site) than on its nature. The magnetic moment on the FIA is close to zero. The local moment on the Fe atoms

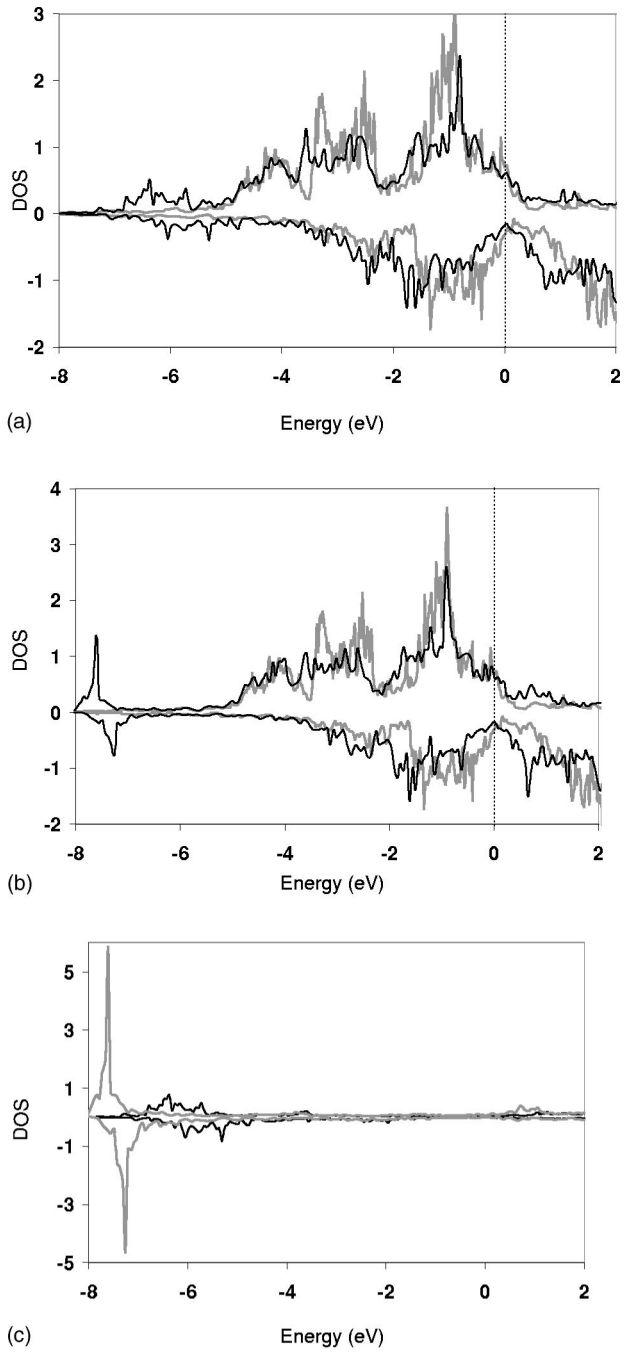

FIG. 2. Local density of states calculated in a bcc supercell containing 54 Fe atoms and one FIA in an octahedral site. Comparison between pure Fe and Fe with an FIA. (a) $s+p+d$ states of an Fe atom 1nn to C; (b) $s+p+d$ states of an Fe atom 1nn to N. The black curves correspond to the Fe atoms 1nn to the FIA, the gray curves to the local density of states of a supercell containing 54 Fe atoms with a bcc structure and no defects; (c) p states of N (gray curve) and C (black curve) in an octahedral site in a bcc structure.

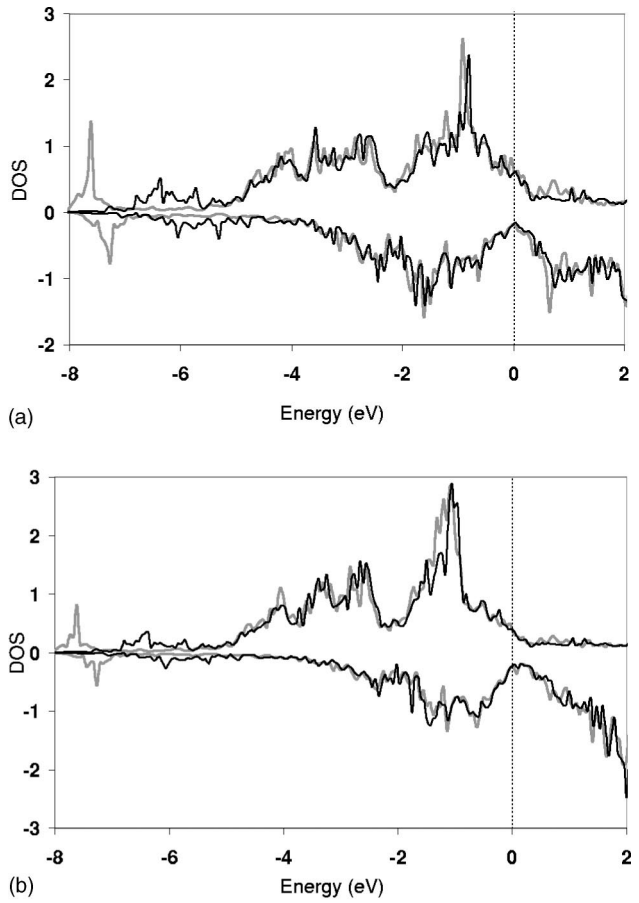

FIG. 3. Local density of states calculated in a bcc supercell containing 54 Fe atoms and one FIA in an octahedral site. Comparison between C and N. (a) $s+p+d$ states of an Fe atom 1nn to C compared to $s+p+d$ states of an Fe atom 1nn to N; (b) $s+p+d$ states of an Fe atom 2nn to C compared to $s+p+d$ states of an Fe atom 2nn to N. The gray curves correspond to the local density of states of the 54-atom supercell containing a N atom. The thin black curves correspond to the local density of states of the 54-atom supercell containing a C atom.

increases with the distance to the FIA, then tends to the local moment of pure Fe. The closest Fe atoms to the FIA experience a very strong moment decrease, while on Fe atoms in the further distance [third nearest neighbor (nn) to the (O) site and second nn to the (T) site], the local magnetic mo-

TABLE VII. Local magnetic moments carried by the FIA's and their neighbors in the bcc structure after relaxation. The calculations were done using 128-atom supercells and 27 k points. For the Fe atom in the perfect bcc supercell, the local magnetic moment is $2.37\mu_B$/atom.

Configuration		C (μ_B/atom)	N (μ_B/atom)
Tetrahedral (T)	FIA	−0.14	−0.11
	Fe (1nn)	1.80	1.70
	Fe (2nn)	2.41	2.44
	Fe (3nn)	2.55	2.55
Octahedral (O)	FIA	0.16	−0.10
	Fe (1nn)	1.72	1.73
	Fe (2nn)	2.29	2.30
	Fe (3nn)	2.50	2.52
	Fe (4nn)	2.34	2.36

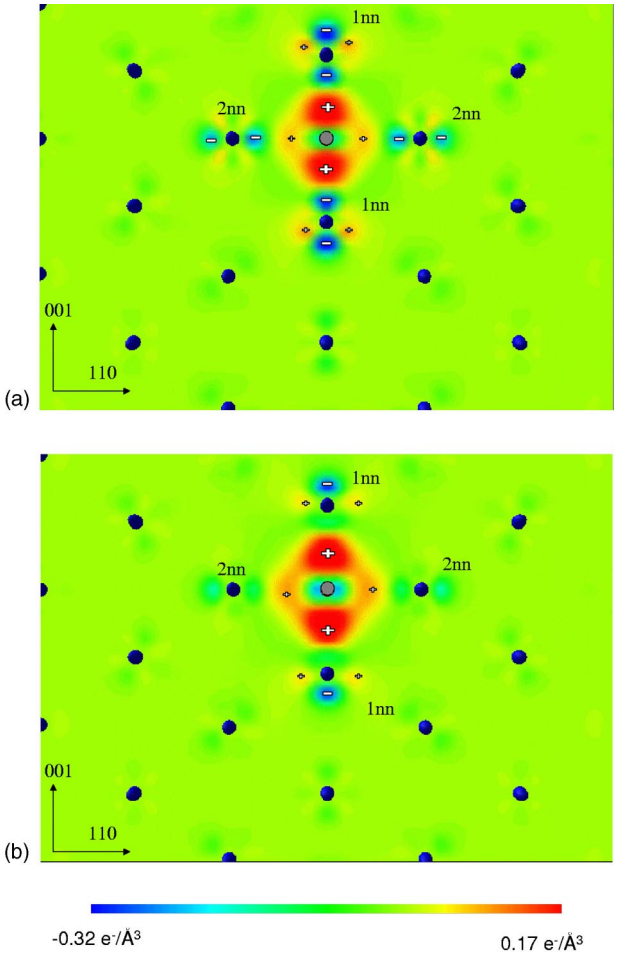

FIG. 4. Electronic density deformation map for one FIA in a 54-atom bcc matrix [$(1\bar{1}0)$ plane]. The black circles are Fe atoms, the gray circles are the FIA's. The + signs indicate regions where the electronic density has increased, while the − signs indicate regions where the density has decreased. (a) The FIA is N, (b) the FIA is C. The units are eV per Å^3.

ment is enhanced as compared to Fe atoms in a bcc Fe perfect crystal.

Figure 4 represents the electronic deformation map corresponding to the density of states of Fig. 2. In the case of C, the only charge transfer clearly visible is between the FIA and its first neighbors, while for N, both the first and the second neighbors contribute significantly. This indicates that the range of the interaction is larger for a N atom than for a C atom.

IV. FIA INTERACTIONS IN bcc Fe

A. FIA-FIA interactions

When one introduces a second FIA in the Fe matrix, the most stable configuration for both types of FIA appears to be configuration 7 (see Fig. 5) as can be observed in Table VIII which summarizes the results. This indicates that, not surprisingly, the FIA's tend to lie as far away from one another as possible. For N, this is consistent with long-range ordering leading to the formation of α''-$Fe_{16}N_2$ in α'-FeN

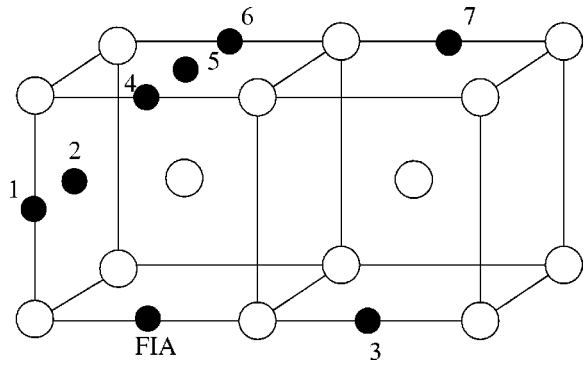

FIG. 5. Possible configurations of two FIA's. Configuration $cfg^i_{V\text{-}FIA_2}$ of Table VIII corresponds to one FIA in the site labeled FIA and the other in the site labeled *i*.

martensite[39] in which configuration 7 is observed. This is also consistent with the experimental observations that in the iron-carbon martensite the carbon atoms are as widely separated as possible.[40] Our results for C are in agreement with the experimental results for which either repulsion or attraction is found depending upon the authors.[41]

Table VIII indicates that the interactions between two identical FIA's appear to be, for the configurations explored here, mostly repulsive for both C and N atoms. Going from 54-atom supercells to 128-atom supercells tends to increase the binding energies as could be expected for calculations involving interstitial atoms. The change is around 0.2–0.3 eV for C atoms and around 0.1–0.2 eV for N FIA's. We thus do not expect dramatic changes in the results of Table VIII when increasing once more the supercell size. Indeed FIA's are smaller than self-interstitial atoms and the effect of the supercell size on self-interstitial atom formation energies in pure Fe was shown to be less than 0.1 eV for supercell sizes larger than 128 atoms and with an empirical potential.[26]

The FIA-FIA interaction can be roughly estimated using the elastic theory, in the same way it was used to estimate the interaction of a FIA with a dislocation.[37] The deformation induced by the FIA is modeled by a tetragonal distortion (characterized by ϵ_{zz} and $\epsilon_{xx}=\epsilon_{yy}$) of the bcc unit cell around the FIA. The elastic interaction is then given by $E_{elast}=-\Sigma_{ij}\sigma_{ij}\epsilon_{ij}a^3$. The displacement field u_i introduced by the point force (oriented along the z direction) is given by[42]

$$u_z=A\left((1-4\nu)\frac{z}{r^3}+\frac{3z^3}{r^5}\right),\quad u_y=-A\left(\frac{y}{r^3}-\frac{3z^2y}{r^5}\right),$$

$$u_x=-A\left(\frac{x}{r^3}-\frac{3z^2x}{r^5}\right). \tag{4.1}$$

The strains ϵ_{ij} and the stresses σ_{ij} and finally the elastic interactions for isotropic bcc Fe were derived from the equations above:

$$\sigma_{ii}=C_{11}\epsilon_{ii}+C_{12}\sum_{j\neq i}\epsilon_{jj}. \tag{4.2}$$

TABLE VIII. Binding energies (in eV) between two FIA's. The calculations were done using 54-atom (respectively 128-atom) supercells and 125 k points (respectively 27 k points). The distances between the two FIA's are in units of lattice parameter. The seventh column contains the energies determined with the elastic theory model described in the text. The eighth column gives the unrelaxed distances between the FIA's, in units of lattice parameter.

Configuration	C-C (54 atoms)	C-C (128 atoms)	N-N (54 atoms)	N-N (128 atoms)	Johnson[a]	E_{elast}	d(FIA-FIA) (a_0)
$cfg^1_{FIA_2}$	−0.94	−0.65	−1.19	−1.05		−0.25	$\sqrt{2}/2$
$cfg^2_{FIA_2}$	−0.42	−0.09	−0.55	−0.40	+0.13	+0.08	$\sqrt{3}/2$
$cfg^3_{FIA_2}$	−2.28	−1.67	−3.03	−1.68		−0.30	1
$cfg^4_{FIA_2}$	−0.17	−0.09	−0.27	−0.33	+0.11	+0.03	1
$cfg^5_{FIA_2}$	−0.14	+0.13	−0.28	−0.16	+0.08	+0.07	$\sqrt{5}/2$
$cfg^6_{FIA_2}$	−0.20	+0.14	−0.29	−0.10		+0.01	$\sqrt{2}$
$cfg^7_{FIA_2}$	−0.09	+0.16	−0.12	−0.03		+0.01	$\sqrt{3}$

[a]Reference 10.

We took experimental data for the pure bcc Fe elastic constants ($C_{11}=240$ GPa, $C_{12}=140$ GPa, $\nu=0.3$) and adjusted A such that $\epsilon_{zz}=\Delta d_1/d_1^0$, i.e., $A=0.125$ Å^3.

This method gives only rough estimation of the FIA-FIA interaction, as we assumed that (i) the introduction of the FIA's leads to an elastic response of the material; (ii) the presence of the FIA does not change significantly the elastic constants; (iii) the deformation is localized on a single bcc unit cell only (with volume a^3). As a consequence no distinction was made between C and N, which are very similar in size. The values obtained with this approach are compared to the *ab initio* results in Table VIII. As expected, the interaction energies obtained with the double-force model described above are underestimated. However, the predictions give the correct trends among the different configurations of Fig. 5. A typical example is the big difference in repulsive energies between configurations $cfg^3_{FIA_2}$ and $cfg^4_{FIA_2}$ which is clearly explained in terms of elastic interactions only, as the distance between FIA's in both configurations is the same. Furthermore the predictions of this elastic model are in rather good agreement with the calculations of Johnson *et al.*,[10] who found that $cfg^2_{FIA_2}$ is the most stable position. It may be worth noticing that Johnson's potential does not take into account the C-C interactions, and his results reflect only the interactions of the local strains near the two C atoms. Therefore it is not surprising that Johnson's results are close to the predictions of this elastic model.

For all the configurations investigated, it appears that the C-C interactions are always less repulsive than the N-N interactions even though the C atoms are ''bigger'' than the N atoms. This may come from the fact that the Fe-C interaction appears to be less localized in energy (Fig. 2). Furthermore, the fact that the elastic predictions and the *ab initio* calculations give different binding energies indicates clearly that the nature of the FIA contributes a lot to the interaction energy.

Keefer and Wert have studied the clustering of carbon and nitrogen in α-Fe using anelastic techniques. Their data for nitrogen suggest the existence of pairs of nitrogen atoms, for which they report a binding energy of 0.07 eV.[43] However in their experiment, there is no indication of the relative positions of the FIA's and their results cannot be directly compared with these calculations.

$cfg^3_{FIA_2}$ for both species is the most repulsive configuration (the least stable) because the two octahedral sites containing the FIA's are on top of each other, aligned along the shortest direction of the site, and thus along the most dilated direction.

Figure 6 represents the local magnetic moments for configurations 1 and 7 on the Fe atoms close to the carbon FIA's, while Fig. 7 represents the local magnetic moment for the same configurations on the Fe atoms close to nitrogen FIA's. The data have been calculated for a 54-atom supercell, but we checked that no real changes occur when going from a 54-atom supercell to a 128-atom supercell. A differentiation is now more visible between C and N on the local moments

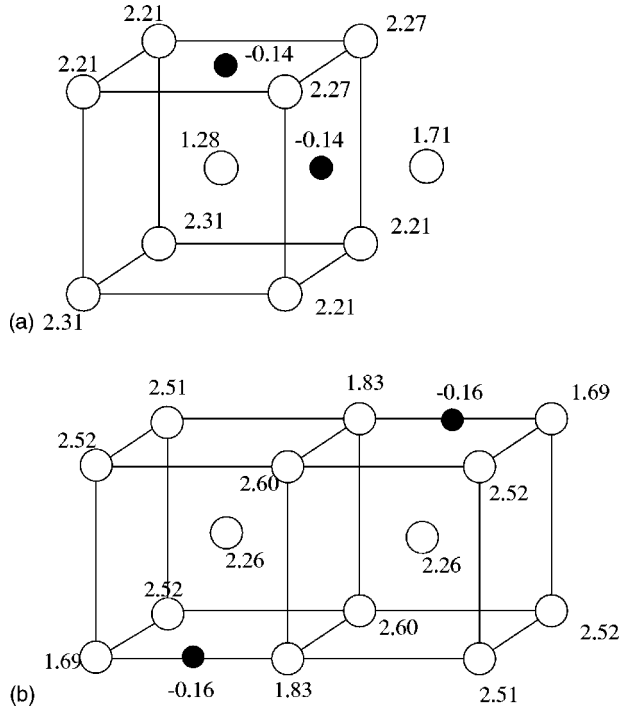

FIG. 6. Local magnetic moments for two C atoms in bcc Fe. The local magnetic moments are given in μ_B. They were obtained in 54-atom unit cells. (a) is configuration $cfg^1_{FIA_2}$ in Table VIII, (b) is configuration $cfg^7_{FIA_2}$ in the same table.

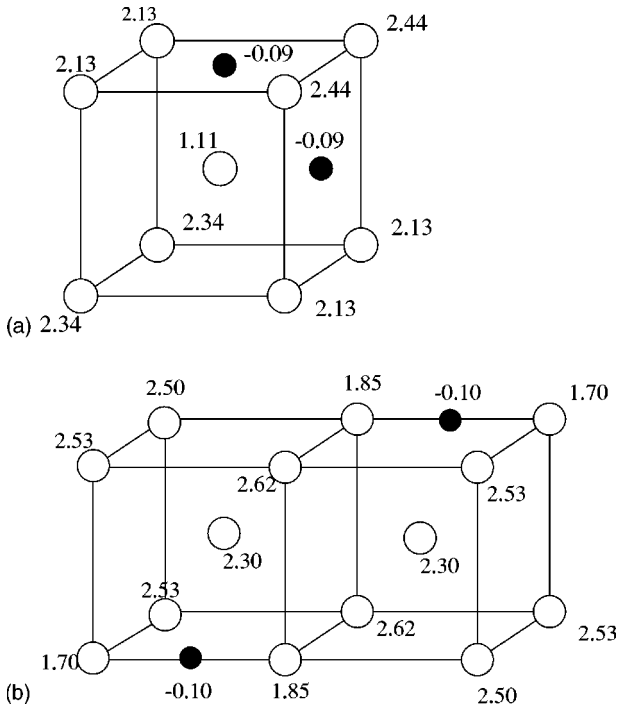

FIG. 7. Local magnetic moments for two N atoms in bcc Fe. The local magnetic moments are indicated in μ_B. They were obtained in 54 atom unit cells. (a) is configuration $\mathrm{cfg}^1_{FIA_2}$ in Table VIII, (b) configuration is $\mathrm{cfg}^7_{FIA_2}$ in the same table.

carried by their neighbor Fe atoms as compared to when a single FIA is present. The most significant case being configuration $\mathrm{cfg}^1_{FIA_2}$. The highest magnetic moment is observed on $\mathrm{cfg}^7_{FIA_2}$ for the N-N interactions. These differences indicate that chemical effects are indeed significant.

B. Interactions of one FIA with one vacancy

Table IX summarizes the binding energies of a C or a N atom situated close to a vacancy. In addition to the two configurations where the FIA is first (configuration $\mathrm{cfg}^1_{V\text{-}FIA}$) and second (configuration $\mathrm{cfg}^2_{V\text{-}FIA}$) neighbor to the vacancy, we also investigated the configuration where the FIA is in the vacancy, i.e., in substitutional position (configuration $\mathrm{cfg}^3_{V\text{-}FIA}$) as well as when the FIA is midway between the vacancy and its first nearest-neighbor atom along the $\langle 111 \rangle$ direction (configuration $\mathrm{cfg}^4_{V\text{-}FIA}$). These four configurations are represented in Fig. 8.

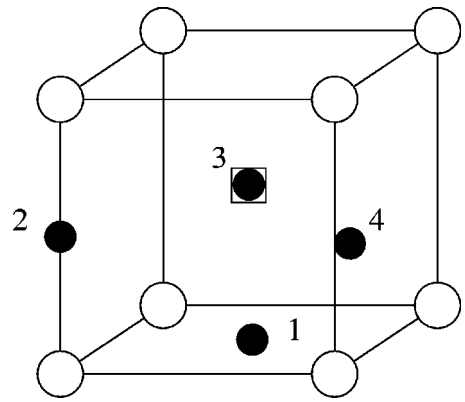

FIG. 8. Four possible positions for a FIA close to a vacancy. The vacancy is represented by a white square. The FIA in the site labeled i corresponds to $\mathrm{cfg}^i_{V\text{-}FIA}$ of Table IX.

The results support the fact that C (respectively N) near a vacancy does not become ''substitutional'' and that $d_{C\text{-}V}$ (respectively $d_{N\text{-}V}$) does not vanish. This is coherent with positron annihilation studies which found that the C atom is at about $0.365a_0$ (instead of $0.5a_0$ in the unrelaxed position) from the vacancy center,[44] where a_0 is the equilibrium lattice parameter. Similar to what was obtained with empirical potentials,[10] the atomic relaxations of the C and N atoms are towards the vacancy. Furthermore, the relaxation of the FIA towards the vacancy is larger for C than for N.

When a vacancy and a FIA interact, they can form a stable V-FIA pair due to trapping effects. Our data indicate that configuration $\mathrm{cfg}^3_{V\text{-}FIA}$ is not a stable configuration, thus the

TABLE IX. Vacancy-interstitial impurity binding energies E_b (in eV). The calculations were done using 54-atom supercells and 125 k points, and 128-atom supercells and 27 k points. The distances are in units of lattice parameter (a_0).

Configuration	C (54 atoms)		C (128 atoms)		N (54 atoms)		N (128 atoms)	
	E_b (eV)	$d_{C\text{-}V}$ (a_0)	E_b (eV)	$d_{C\text{-}V}$ (a_0)	E_b (eV)	$d_{N\text{-}V}$ (a_0)	E_b (eV)	$d_{N\text{-}V}$ (a_0)
$\mathrm{cfg}^1_{V\text{-}FIA}$	0.44	0.40	0.47	0.41	0.67	0.45	0.71	0.45
$\mathrm{cfg}^2_{V\text{-}FIA}$	−0.09	0.64	−0.01	0.64	0.14	0.72	0.20	0.70
$\mathrm{cfg}^3_{V\text{-}FIA}$	−0.33	0			−0.88	0		
$\mathrm{cfg}^4_{V\text{-}FIA}$	−0.11	0.24			−0.44	0.28		
Johnson *et al.*[a] ($\mathrm{cfg}^1_{V\text{-}FIA}$)	0.41	0.35						
Rosato *et al.*[b] ($\mathrm{cfg}^1_{V\text{-}FIA}$)	0.48							
Experimental	0.41[c]	0.365[d]						

[a]Reference 10.
[b]Reference 11.
[c]Reference 46.
[d]Reference 44.

TABLE X. FIA migration energy when bound to a vacancy (in eV), and vacancy (V) migration energy when bound to a FIA. The calculations were done using 54-atom supercells and 8 k points (Ref. 52). A set of configuration has been built along the transition path, and each one has been relaxed keeping the FIA position fixed along the migration path.

Configuration	C	N
FIA $(O)_{1nn} \rightarrow (O)_{1nn}$	0.4	1.0
FIA $(O)_{1nn} \rightarrow (O)_{2nn}$	0.6	1.0
FIA $(O)_{2nn} \rightarrow (O)_{1nn}$	0.1	0.4
V 1nn $\rightarrow$ 2nn	0.5	0.76
V 2nn $\rightarrow$ 1nn	0.3	0.2

migration path of this V-FIA complex between two $\mathrm{cfg}^1_{V\text{-}FIA}$-type configurations does not go through the $\mathrm{cfg}^3_{V\text{-}FIA}$, i.e., the vacant site. The FIA may migrate from one $(O)_{1nn}$ site ($\mathrm{cfg}^1_{V\text{-}FIA}$) to the next nearest one by two other possible paths: a direct path, or a path going through the $\mathrm{cfg}^2_{V\text{-}FIA}(O)_{2nn}$ configuration.

These migration energies have been evaluated, using 54-atom supercells and $8k$ points.[52] A set of configurations was built along the possible transition path; each configuration was relaxed fixing the FIA position along the migration path. The results of these calculations appear in Table X. Within the accuracy of these results, the two possible paths appear to have similar activation energies. However for both possible transition paths, the activation energies appear to be higher for N than for C, in contrast with the migration energies of isolated N and C atoms in bcc Fe as can be seen in Table II. These results are however consistent with the fact that N atoms have a stronger binding energy with vacancies than C atoms. The stronger binding energy of N with one vacancy associated with a lower mobility of the V-N complex indicates that the trapping effect of N atoms on vacancies is greater than the trapping effect of C atoms on vacancies.

To complete this study on trapping effects, the migration energy of the vacancy from a site first nearest neighbor to the FIA towards a site second nearest neighbor to the FIA was evaluated, as well as the reverse jump (i.e., from the second nearest-neighbor site to the first nearest-neighbor site). The two migration energies are reported in Table X. Despite the large V-FIA binding energy the vacancy migration energy to move away from the FIA to a second nearest neighbor is close to the migration energy of the vacancy in pure Fe. Meanwhile, the migration energy from the second nearest-neighbor to the first nearest-neighbor position is rather low. This indicates that the vacancy moves easily away from the FIA, but it comes back more easily close to the FIA.

The results for the vacancy-C binding energy are in good agreement with the data obtained by Johnson *et al.*,[10] Beeler[45] or by Rosato[11] with empirical potentials. However the comparison with experimental results is not straightforward as they are not always very coherent and arise from different techniques. Arndt and co-workers[46] examining a neutron-irradiated Fe found by calorimetric measurements a large binding energy (0.41 eV) of C with a defect, which they postulate to be probably a vacancy. However, Wuttig *et al.*[47] examined by magnetic measurements the carbon and nitrogen trapping in Fe following low-temperature electron and neutron irradiations. They concluded that interstitial clusters formed during the low-temperature neutron irradiation acted as traps for carbon and nitrogen atoms, whereas vacancies were the trapping defects following electron irradiation. Little and Harries[5] also consider that the binding energy measured by Arndt and co-workers[46] very likely corresponds to the binding energy of carbon to an interstitial cluster. On the other hand, Takaki *et al.*[32] doing careful resistivity measurements in very pure Fe and C doped Fe following low-temperature electron irradiation estimate that the binding energy of a carbon atom with a vacancy is 1.1 eV, while Vehanen *et al.*[2] doing positron-lifetime measurements on electron-irradiated high purity and C doped Fe find 0.85 eV. Furthermore, in our calculations, a N atom tends to have a stronger interaction with a vacancy than a C atom with a vacancy in contrast with the interpretation of Wuttig *et al.*[47] of their experimental data leading to the conclusion that the C-vacancy binding energy is stronger than the N-vacancy binding energy. Later Mondino and Seeger[48] also observe that N-V pairs dissociate more easily than C-V pairs.

C. Interactions of two FIA's with one vacancy

The possible configurations for one vacancy and two FIA's (first neighbors to the vacancy) are represented in Fig. 9. In addition to the two obvious configurations which correspond to the two FIA's being first neighbors to the vacancy (in agreement with the very strong binding energy) and aligned either along the $\langle 110 \rangle$ direction (configuration $\mathrm{cfg}^1_{FIA_2}$) or along the $\langle 001 \rangle$ direction (configuration $\mathrm{cfg}^2_{FIA_2}$), we also considered a case where the two FIA's are second neighbors of the vacancy and aligned along the $\langle 110 \rangle$ direction (configuration $\mathrm{cfg}^3_{FIA_2}$) as well as when the two FIA's are aligned along the $\langle 111 \rangle$ direction, thus forming a sort of $\langle 111 \rangle$ dumbbell (configuration $\mathrm{cfg}^4_{FIA_2}$). In addition to the configurations described above, two configurations where one FIA is in an octahedral site first nearest neighbor of the vacancy and the second one is in an octahedral site second nearest-neighbor site have been considered, configurations $\mathrm{cfg}^5_{FIA_2}$ and $\mathrm{cfg}^6_{FIA_2}$ of Fig. 9.

For a given configuration, the FIA position can be described in terms of coordinates relative to the vacancy positioned at the origin of the space, i.e., at (1,0,0). With this notation, in $\mathrm{cfg}^1_{FIA_2}$ the FIA positions are $(0,0,-a/2)$ and $(a/2,0,0)$. This notation will be used in the last part of this paper.

The binding energy of one vacancy with two FIA's was determined using Eq. (2.4) and summarized in Table XI. As expected from geometric considerations and the results from Table IX the most stable configurations, i.e., the ones with the strongest binding energies, are those where both FIA's occupy first nearest-neighbor octahedral sites.

Interestingly enough, C and N do not exhibit the same behavior and do not have the same most stable configuration. While the C atoms prefer to be in two octahedral sites the closest to each other, i.e., $\mathrm{cfg}^1_{FIA_2}$, the N atoms are more

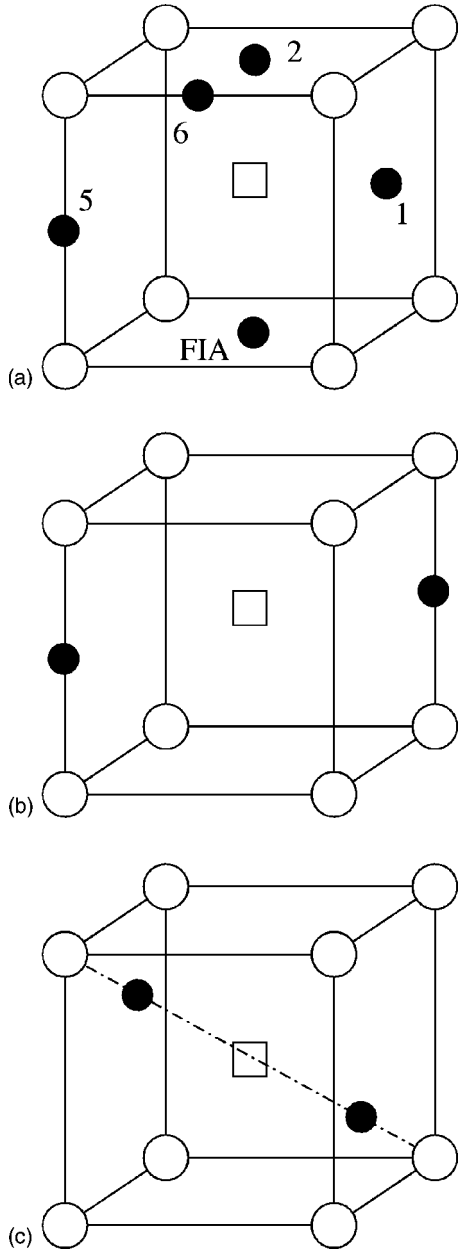

FIG. 9. Possible configurations for FIA-FIA interactions with one vacancy. (a) Configuration $cfg^{i}_{V\text{-}FIA_2}$ of Table XI corresponds to one FIA in the site labeled FIA and the other in the site labeled *i*. (b) is $cfg^{3}_{V\text{-}FIA_2}$, (c) is $cfg^{4}_{V\text{-}FIA_2}$ in the same table.

stable when they occupy two octahedral sites symmetric with reference to the vacancy position along a ⟨100⟩ direction which corresponds to configuration $cfg^{2}_{FIA_2}$.

When the two FIA's are aligned along the ⟨100⟩ direction, there is almost no interaction between them, and the resulting binding energy is close to what would be obtained by the superposition of two V-FIA complexes without interaction between the two complexes: (i) The relaxation of each FIA towards the vacancy is close to the relaxation of a single FIA towards the vacancy; (ii) the binding energy of the vacancy with the two FIA's can be roughly obtained by taking twice the binding energy of one of the V-FIA complexes; (iii) the electronic structure due to each FIA is similar to the one obtained for a simple V-FIA as can be seen in the electronic density deformation map in Fig. 10.

TABLE XI. Binding energies (in eV) of one vacancy with two FIA's. The reference state for the binding energies is the energy of a system where none of the non-Fe atoms (i.e., the vacancy or the FIA's) interact. The calculations were done using 54-atom supercells and 27 *k* points. For the two configurations where the FIA are both first neighbor to the vacancy, the calculations have been done also with 128-atom supercells and 27 *k* points. The error on the binding-energy calculations done with only a 54-atom supercell can thus be estimated to be around 20%.

Configuration	C (54 atoms)	C (128 atoms)	N (54 atoms)	N (128 atoms)
$cfg^{1}_{V\text{-}FIA_2}$	1.24	1.50	0.32	0.46
$cfg^{2}_{V\text{-}FIA_2}$	0.71	1.07	1.25	1.54
$cfg^{3}_{V\text{-}FIA_2}$	−0.27		0.10	
$cfg^{4}_{V\text{-}FIA_2}$	0.77		−2.09	
$cfg^{5}_{V\text{-}FIA_2}$	−0.14		0.46	
$cfg^{6}_{V\text{-}FIA_2}$	0.30		0.85	

In contrast to the case above, when the two FIA's are aligned along the ⟨110⟩ direction, N and C atoms behave differently. For N, the two N atoms sit in positions close to the equilibrium position of two simple V-FIA complexes; this is very probably due to the strong repulsion between N FIA's (see Table VIII) and the distance between them is 2.29 Å compared to the distance of 2.02 Å between two octahedral sites. The octahedral sites are thus slightly distorted, which leads to a lower binding energy, and a dissymmetric interaction of each FIA with its four second nearest-neighbor Fe atoms; two of these neighbors are shared by each FIA.

For C, despite the metallic environment due to the Fe atoms, a C-C covalent bond is formed. The distance between the two C atoms is 1.42 Å which is the typical covalent bond length of C (1.38–1.48 Å for sp^2 bonds[49]). This covalent bond leads to a high binding energy, and the electronic density deformation map shows the high electronic concentration between the two C atoms (Fig. 11). Such a covalent bonding does not appear when the two FIA's are N atoms. This covalent bonding makes the local moments of the Fe atoms the closest to the octahedral site increase to $2.43\mu_B$, while the moment of the Fe atoms close to the two N atoms decreases significantly to $1.39\mu_B$, as can be seen in Fig. 12.

These results can be interpreted in terms of the alignment of the octahedral cells formed by the six Fe atoms around the FIA's. When the FIA is a C atom, the octahedral cells containing the C atoms appear to favor configurations where they are orthogonal to each other, whereas for N atoms the octahedral cells tend to arrange themselves in a manner similar to what is observed in ordered $Fe_{16}N_2$.

The difference between the binding energy of two FIA's with a vacancy (from Table XI) and the binding energy of one FIA with a vacancy (from Table IX) gives the energy needed to add a FIA to a FIA-vacancy pair already formed. Our data (compare Table XI with Table IX) indicate that for

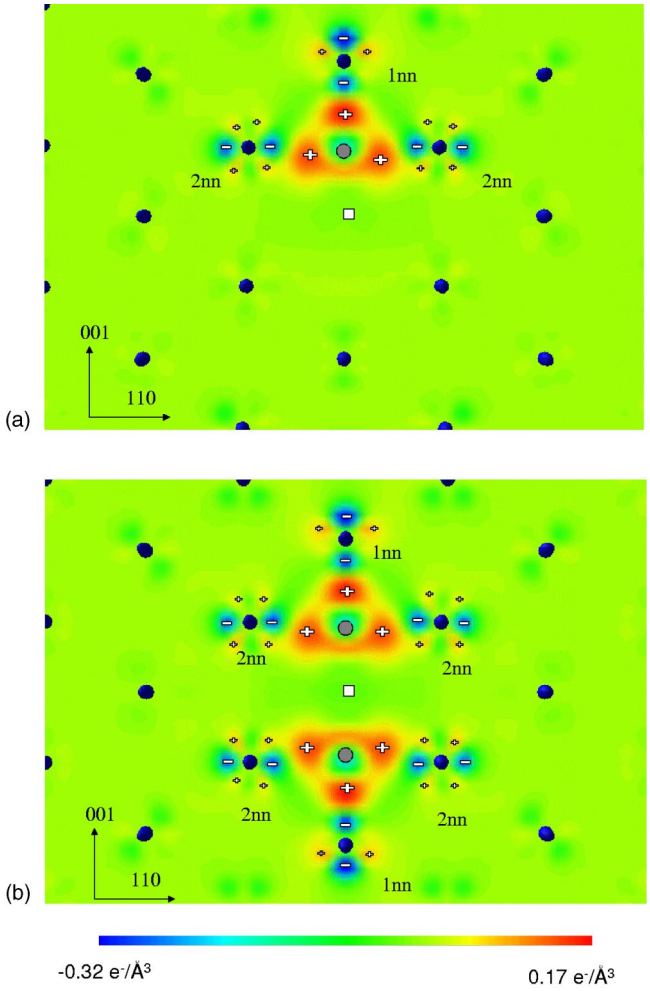

FIG. 10. Electronic density deformation map [$(1\bar{1}0)$ plane] for one N FIA close to one vacancy compared to the electronic density deformation map for two N FIA's and one vacancy all aligned along the $\langle 001 \rangle$ direction (configuration $cfg^2_{V\text{-}FIA_2}$ of Table XI). The + signs indicate regions where the electronic density has increased, while the − signs indicate regions where the density has decreased. The units are eV per Å^3.

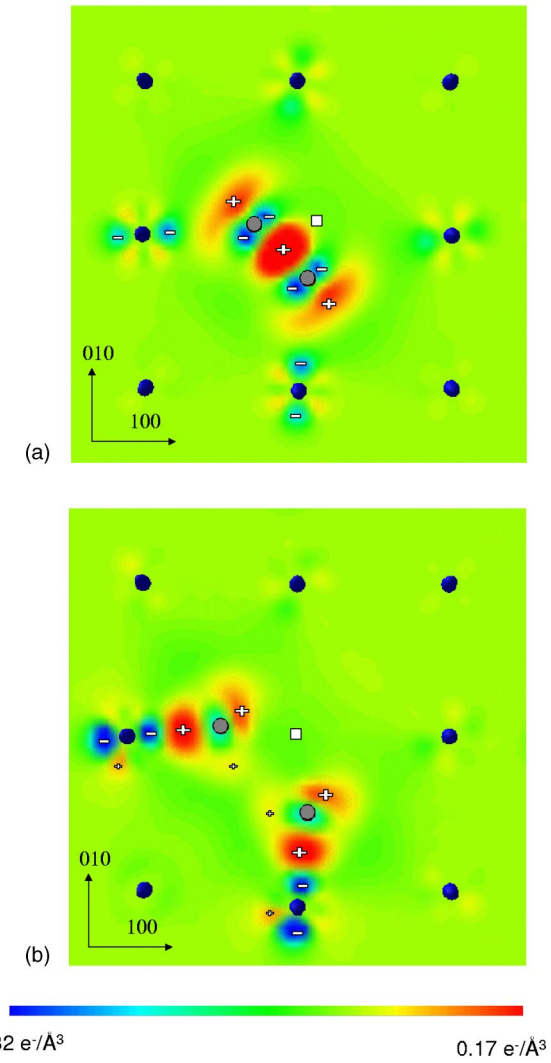

FIG. 11. Electronic density deformation map for two FIA's close to one vacancy. The + signs indicate regions where the electronic density has increased, while the − signs indicate regions where the density has decreased. (a) is configuration $cfg^1_{V\text{-}FIA2}$ for two C atoms [(001) plane]. (b) is the same configuration for two N atoms. The units are eV per Å^3.

C, it is preferable to add a C atom to an already formed C-V pair than to form a new C-V pair in agreement with Weller study on Snoek peak of interstitial foreign atoms and their complexes in bcc metals.[50] Our results are also in agreement with Takaki's findings[32] that monovacancies are nuclei for small clusters containing a limited amount of C atoms. These results are, however, in contradiction with the kinetics discussed in (Ref. 46) which are clearly bimolecular, indicating that only one carbon atom associates with each vacancy and with our results. For N, the data are not so clear. Indeed the difference between the binding energy of two N atoms with one vacancy and the binding energy of one N atom with a vacancy is very close to (for 54 atoms) and even lower than (for 128 atoms) the binding energy of one N atom to a vacancy. These results indicate that for N there exists very probably a competition between the formation of another N-V pair and the formation of a V-N_2 triplet. Indeed Weller's study indicates that N are found only as V-N pairs. Under normal conditions and even under irradiation, the vacancy concentration in Fe is smaller than the N or C atom concentration (for pure Fe or Fe alloys), and a large proportion of the vacancies may be associated to one or two FIA's, with strong binding energies.

TABLE XII. Binding energies (in eV) of one vacancy with three FIA's. The reference state for the binding energies is the energy of a system where none of the non-Fe atoms (i.e., the vacancy or the FIA's) interact. The calculations were done using 54-atom supercells and 125 *k* points (or 128-atom supercells and 27 *k* points).

Configuration	C (54 atoms)	C (128 atoms)	N (54 atoms)	N (128 atoms)
$cfg^1_{V\text{-}FIA_3}$	0.21	0.72	−0.74	−0.46
$cfg^2_{V\text{-}FIA_3}$	1.24	1.84	−0.38	−0.11

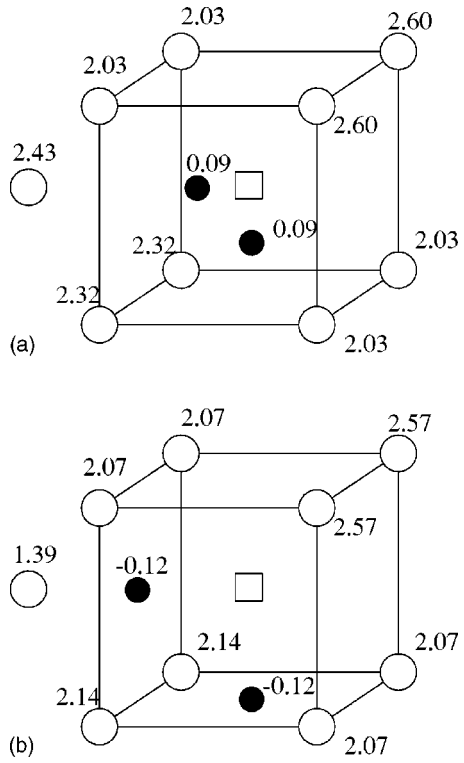

FIG. 12. Local magnetic moments, in μ_B, for $\mathrm{cfg}^1_{V\text{-}FIA_2}$ of Table XI. They were obtained using 54-atom supercells. (a) the FIA's are C atoms, (b) the FIA's are N atoms.

An estimation of the binding energy of complexes containing three FIA's and one vacancy seems to indicate that there is no significant binding energy for the third C atom (Table XII). For the two configurations investigated, the FIA positions were $(0,a/2,0)$, $(0,0,-a/2)$, and $(0,0,a/2)$ for $\mathrm{cfg}^1_{FIA_3}$, and $(a/2,0,0)$, $(0,a/2,0)$, $(0,0,a/2)$ for $\mathrm{cfg}^2_{FIA_3}$. The results indicate that the less unfavorable situation is when three C atoms are bound to a vacancy. The corresponding binding energy is 1.24 eV for 54 atoms and 1.84 for 128 atoms, which indicates that there is no significant binding for the third C atom as compared to the first two. Nevertheless, if the vacancy concentration is low, the formation of some $V\text{-}C_3$ complexes can be expected as the binding energy of the third C atom is around 0.3 eV (for 128-atom supercell results). For N the situation is much less favorable, as can be expected from the binding energies of the two $V\text{-}N_2$ configurations studied previously. Therefore, we expect the formation of $V\text{-}N_3$ complexes to be highly improbable.

D. FIA–self-interstitial atom interactions

Finally we looked at the interactions of N or C atoms with self-interstitial atoms. Indeed, according to Little and Harries,[5] nitrogen interstitial atoms reduce the jump frequency of the self-interstitial atom by a factor of 4×10^4 at 50 °C and thus drastically affect the long-range migration behavior of the self-interstitial atom point defects. As a result self-interstitial atom clusters formed under irradiation nucleate on a much finer scale than in the absence of nitrogen.

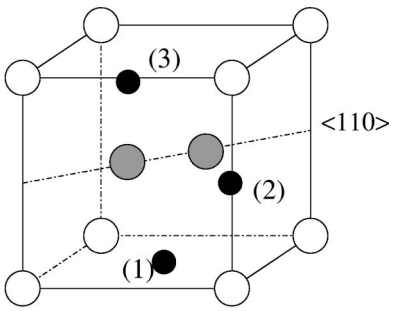

FIG. 13. FIA positions relative to the ⟨110⟩ SIA. (1) corresponds to $\mathrm{cfg}^1_{SIA\text{-}FIA}$ of Table XIII, (2) to $\mathrm{cfg}^2_{SIA\text{-}FIA}$, and (3) to $\mathrm{cfg}^3_{SIA\text{-}FIA}$.

Takaki and co-workers[32] estimate the binding energy between a self-interstitial atom and a carbon atom to be 0.11 eV. Earlier on, Johnson *et al.*[51] calculated that an attractive binding energy of 0.5 eV existed between the ⟨110⟩ dumbbell and a carbon atom (Fig. 12).

We have investigated the possible interactions between the most stable self-interstitial in Fe, the ⟨110⟩ dumbbell and C as well as N impurities. A ⟨110⟩ dumbbell was introduced in a supercell. All the atoms were relaxed using the conjugate gradient algorithm and the energy of this relaxed system was determined. In this relaxed supercell, a C or N atom was placed at different sites labeled $\mathrm{cfg}^1_{SIA\text{-}FIA}$, $\mathrm{cfg}^2_{SIA\text{-}FIA}$, and $\mathrm{cfg}^3_{SIA\text{-}FIA}$ in Fig. 13. The new system was then relaxed once more using the conjugate gradient algorithm and the new energy determined. The binding energies [calculated using Eq. (2.3)] corresponding to the different positions presented in Fig. 13 are summarized in Table XIII. Despite some possible supercell size effects, the FIA self-interstitial atom interactions appear to be repulsive or if they become attractive in a bigger supercell the interaction should remain small and in any case not as large as the FIA-vacancy interactions. This is in disagreement with Johnson's calculated results or with Takaki experimental work.

In our results, this repulsion is larger for the N atoms than for the C atoms, the difference being more visible for configuration $\mathrm{cfg}^1_{SIA\text{-}FIA}$, while Little and Harries[5] observe that it is probable that the binding energy of the self-interstitial atom to N is similar to that of the self-interstitial atom to C. The discrepancy with the experimental results may come from the fact that no indication is given about the relative position and distance of the C from the dumbbell. Indeed, for configuration $\mathrm{cfg}^3_{SIA\text{-}FIA}$, there is not much difference whether the FIA is a C or a N atom. Moreover, it can be noticed that the repulsion between C and N with the ⟨110⟩ dumbbell is for some configuration smaller than the energy difference between the ⟨111⟩ crowdion and the ⟨110⟩ dumbbell [$\simeq$0.7 eV (Ref. 26)]. These preliminary results indicate thus that the stability of the ⟨110⟩ dumbbell may not be affected by the presence of C or N FIA. However the interaction of FIA's with self-interstitial atom clusters needs to be further explored.

E. Summary

We have determined the binding energy of C and N atoms with intrinsic point defects as well as with other FIA's of the

TABLE XIII. ⟨110⟩ dumbbell binding energies (in eV) with impurities situated in the positions defined in Fig. 13. The calculations were carried out using 54-atom supercells and 125 *k* points, and 128-atom supercells and 27 *k* points.

Position	C (54 atoms)	C (128 atoms)	N (54 atoms)	N (128 atoms)	C (Johnson *et al.*[a])
$cfg^1_{SIA\text{-}FIA}$	−0.39	−0.19	−0.73	−0.58	+0.56
$cfg^2_{SIA\text{-}FIA}$	−0.58	−0.31	−0.86		
$cfg^3_{SIA\text{-}FIA}$	−0.32	−0.09	−0.35	−0.18	

[a]Reference 10.

same type. Our results indicate that there is a strong binding energy of C and N to the vacancy. This binding energy is greater when the FIA is a N atom than when it is a C atom. Because of this large binding energy the migration energy of a N atom associated with a vacancy is lower than the migration energy of a C atom associated with a vacancy. The trends are opposite when no vacancies are present. Point defects affect thus very strongly the behavior of interstitial impurities, which can explain the discrepancies observed in the literature. Furthermore many experimental data are not directly comparable to our calculations and are obtained through a model. For instance, positron-lifetime experiments give the dissociation enthalpy, i.e., the sum of the binding energy and of the migration energy of the fastest species. Depending upon what one chooses as the experimental vacancy migration energy, the deduced experimental binding energy changes. Our data indicate also that when two FIA's are close to each other in an Fe matrix, some configurations lead to a repulsion of the FIA's, repulsion which can be overcome by the presence of vacancies. The repulsion between the N atoms is always more significant than the repulsion between C atoms. As a result, when a vacancy is introduced close to two C atoms, a covalent bonding forms while no such bonding appears between N atoms. Under irradiation, numerous vacancies and self-interstitial atoms are introduced in the matrix, and our results indicate clearly how the presence of N or C atoms can affect the microstructure evolution even if some results are only trends.

V. CONCLUSIONS

Some of the known properties of C and N impurity atoms in α-Fe are correctly reproduced by our *ab initio* calculations. In particular, (i) the impurity C and N atoms occupy octahedral rather than tetrahedral sites; (ii) the tetrahedral site corresponds to the saddle point for N and C migration, and the migration energy is equal to the energy difference between the octahedral and tetrahedral sites; (iii) the experimental migration energy of the FIA's in α-Fe is very close to the *ab initio* values, and this is true also for the diffusivity prefactor; (iv) the binding energy of a vacancy with a C atom is strong and is very close to the experimental results.

As a consequence, the formation of carbon-vacancy or nitrogen-vacancy complexes can be a good explanation for the difficulty to obtain coherent data on vacancy properties which are masked by the complexes.

In complement, some important results have been obtained.

(i) A vacancy can bind to up to two FIA's only.

(ii) The interactions between two FIA's are mostly repulsive except in a few particular cases. When a vacancy is introduced, an attractive interaction builds up between the two FIA's and the vacancy. In the case of C atoms a covalent C-C bond forms.

(iii) C atoms tend to occupy octahedral sites whose shortest distances are perpendicular to each other, while N atoms appear to favor the alignment of the octahedral sites so that the shortest distances are parallel to each other.

(iv) No attraction between FIA's and ⟨110⟩ self-interstitial atoms have been observed. At short distance, a repulsion of a few tenth of eV has been obtained.

Finally, C and N have similar properties, in terms of the migration energies, binding energies with a vacancy, or binding energy with a self-interstitial atom. The migration energy of the FIA is slightly smaller for N which is a smaller atom, on the other hand the binding energy with a vacancy is slightly smaller for C. Nevertheless, the complexes formed by one single vacancy and two FIA's behave differently whether the FIA is a carbon or a nitrogen atom.

The data obtained by *ab initio* calculations appear thus to be useful to analyze the behavior of point defects in the presence of foreign interstitial atoms. Similar calculations on the C-N interactions are under way.

ACKNOWLEDGMENTS

Regular and fruitful discussions with our colleague A. Legris are greatly acknowledged. This work was part of the EDF REVE (virtual reactor) project which aims at simulating the irradiation effects in structural materials. This research was supported by the C.I.N.E.S. and I.D.R.I.S. French national computational centers as well as by the C.R.I. of the U.S.T.L. supported by the Fonds Européens de Développement Régional. Part of this work was done on the supercomputers at CEA Grenoble in the framework of an EDF-CEA contract. This work is also partially funded by the ITEM European network (FIR1-CT-2001-20136) and the PERFECT European project (FI6O-CT-2003-508840).

[1] H.E. Schaefer, K. Maier, M. Weller, D. Herlach, A. Seeger, and J. Diehl, Scr. Metall. **11**, 803 (1977).
[2] A. Vehanen, P. Hautojärvi, J. Johansson, J. Yli-Kauppila, and P. Moser, Phys. Rev. B **25**, 762 (1982).
[3] Ahn Hardouin du Parc, Ph.D. thesis, Paris XI-Orsay University, CEA Report No. CEA R 5791, 1998.
[4] E.A. Little, Int. Met. Rev. **204**, 25 (1976).
[5] E.A. Little and D.R. Harries, Met. Sci. J. **4**, 188 (1970).
[6] H. Wagenblast and A.C. Damask, J. Phys. Chem. Solids **23**, 21 (1961).
[7] F.E. Fujita and A.C. Damask, Acta. Metall. **12**, 331 (1964).
[8] C.S. Becquart, C. Domain, A. Legris, and J.C. Van Duysen, J. Nucl. Mater. **280**, 73 (2000).
[9] G.J. Ackland, D.J. Bacon, A.F. Calder, and T. Harry, Philos. Mag. A **75**, 713 (1997).
[10] R.A. Johnson, G.J. Dienes, and A.C. Damask, Acta Metall. **12**, 1215 (1964).
[11] V. Rosato, Acta Metall. **37**, 2759 (1989).
[12] M. Ruda, D. Farkas, and J. Abriata, Scr. Mater. **46**, 349 (2002).
[13] F. Finnis and J.E. Sinclair, Philos. Mag. A **50**, 45 (1984).
[14] V. Rosato, M. Guillope, and B. Legrand, Philos. Mag. A **59**, 321 (1989).
[15] P. Hohenberg and W. Kohn, Phys. Rev. **136**, 864 (1964); W. Kohn and L. Sham, Phys. Rev. B **140**, 1133 (1965).
[16] J. Hafner, Acta Mater. **48**, 71 (2000).
[17] G. Kresse and J. Hafner, Phys. Rev. B **47**, 558 (1993); **49**, 14 251 (1994).
[18] G. Kresse and J. Furthmüller, Phys. Rev. B **54**, 11 169 (1996).
[19] G. Kresse and J. Furthmüller, Comput. Mater. Sci. **6**, 15 (1996).
[20] D. Vanderbilt, Phys. Rev. B **41**, 7892 (1990); G. Kresse and J. Hafner, J. Phys.: Condens. Matter **6**, 8245 (1996).
[21] J.P. Perdew and A. Zunger, Phys. Rev. B **23**, 5048 (1981).
[22] J.P. Perdew and Y. Wang, Phys. Rev. B **45**, 13 244 (1991).
[23] G. Kresse and D. Joubert, Phys. Rev. B **59**, 1758 (1999); P.E. Blöchl, *ibid.* **50**, 17 953 (1994).
[24] S.H. Vosko, L. Wilk, and M. Nusair, Can. J. Phys. **58**, 1200 (1980).
[25] H.J. Monkhorst and J.D. Pack, Phys. Rev. B **13**, 5188 (1976). In the original Monkhorst and Pack scheme, the k point mesh is always symmetric around the Γ point, whereas very often in our calculations we adopted grids centered at the Γ point.
[26] C. Domain and C.S. Becquart, Phys. Rev. B **65**, 024103 (2002).
[27] G. Simonelli, R. Pasianot, and E.J. Savino, Phys. Rev. B **50**, 727 (1994).
[28] C. Kittel, *Introduction to Solid State Physics*, 6th ed. (Wiley, New York, 1987).
[29] G. Kresse and D. Joubert, Phys. Rev. B **59**, 1758 (1999).
[30] G.K. Williamson and R.E. Smallmann, Acta Crystallogr. **6**, 361 (1953).
[31] A.D. Le Claire, in *Numerical Data and Functional Relationships in Science and Technology*, edited by H. Mehrer, Landolt-Börnstein, New Series, Group III, Vol. 26 (Springer-Verlag, Berlin, 1990), Chap. 8, pp. 480–481.
[32] S. Takaki, J. Fuss, H. Kugler, U. Dedek, and H. Schults, Radiat. Eff. **79**, 87 (1983).
[33] M. Weller and J. Diehl, Scr. Metall. **10**, 101 (1976).
[34] G.H. Vineyard, J. Phys. Chem. Solids **3**, 121 (1957).
[35] D.E. Jiang and E.A. Carter, Phys. Rev. B **67**, 214103 (2003).
[36] A. S. Nowick and B. S. Berry, *Anelastic Relaxation in Crystalline Solids* (Academic Press, New York, 1972), p. 235.
[37] A.W. Cochard, G. Schoek, and H. Wiedersich, Acta Metall. **3**, 533 (1955).
[38] See http://physics.nist.gov/PhysRefData/
[39] P. Rochegude and J. Foct, Phys. Status Solidi A **98**, 51 (1986).
[40] W.K. Choo and R. Kaplow, Acta Metall. **21**, 725 (1973).
[41] R.B. McLellan and C. Ko, Acta Metall. **8**, 2151 (1987).
[42] J.P. Hirth and J. Lothe, *Theory of Dislocation*, McGraw-Hill Series in Material Science and Engineering (McGraw-Hill, New York, 1968).
[43] D. Keefer and C. Wert, Acta Metall. **11**, 489 (1963).
[44] P. Hautojärvi, J. Johansson, A. Vehanen, J. Yli-Kauppila, and P. Moser, Phys. Rev. Lett. **44**, 1326 (1980).
[45] J.R. Beeler, Jr., *Interatomic Potentials and Simulation of Lattice Defects*, edited by P.C. Gehlen and J.R. Beeler, Jr. (Plenum Press, New York, 1972).
[46] R.A. Arndt and A.C. Damask, Acta Metall. **12**, 341 (1964).
[47] M. Wuttig, J.T. Stanley, and H.K. Birnbaum, Phys. Status Solidi **27**, 701 (1968).
[48] M. Mondino and A. Seeger, Scr. Metall. **11**, 817 (1977).
[49] J. March, *Advanced Organic Chemistry* (Wiley, New York, 1985).
[50] M. Weller, Journal de Physique **46**, C10 (1985).
[51] R.A. Johnson and A.C. Damask, Acta Metall. **12**, 443 (1964).
[52] For the calculation of the migration path, it was checked that the results are not dramatically changed when using a $5\times5\times5$ k points mesh.